Rock and Soil Mechanics

Volume 42 | Issue 5 Article 9

9-16-2021

Simulation of debris flow impacting bridge pier tests based on smooth particle hydromechanics method

Heng LIANG
Key Laboratory of Mountain Hazards and Surface Process, Institute of Mountain Hazards and Environment, Chinese Academy of Sciences, Chengdu, Sichuan 610041, China

Ji-lin LI
China State Railway Group Co. Ltd., Beijing 100844, China

Fa-ming LIU
China Railway Eryuan Engineering Group Co. Ltd, Chengdu, Sichuan 610031, China

Lun ZHANG
Chengdu Lanzhou Railway CO., Ltd., Chengdu, Sichuan 610031, China

See next page for additional authors

Custom Citation

LIANG Heng, LI Ji-lin, LIU Fa-ming, ZHANG Lun, FU Gang, LI Ming-qing, HE Si-ming, . Simulation of debris flow impacting bridge pier tests based on smooth particle hydromechanics method[J]. Rock and Soil Mechanics, 2021, 42(5): 1473-1484.

Simulation of debris flow impacting bridge pier tests based on smooth particle hydromechanics method

Authors

Heng LIANG, Ji-lin LI, Fa-ming LIU, Lun ZHANG, Gang FU, Ming-qing LI, and Si-ming HE

Rock and Soil Mechanics 2021 42(5): 1473−1484 ISSN 1000−7598
https: //doi.org/10.16285/j.rsm.2020.6107 rocksoilmech.researchcommons.org/journal

Simulation of debris flow impacting bridge pier tests based on smooth particle hydromechanics method

LIANG Heng[1], LI Ji-lin[2], LIU Fa-ming[3], ZHANG Lun[4], FU Gang[3], LI Ming-qing[3], HE Si-ming[1]

1. Key Laboratory of Mountain Hazards and Surface Process, Institute of Mountain Hazards and Environment, Chinese Academy of Sciences, Chengdu, Sichuan 610041, China
2. China State Railway Group Co. Ltd., Beijing 100844, China
3. China Railway Eryuan Engineering Group Co. Ltd, Chengdu, Sichuan 610031, China
4. Chengdu Lanzhou Railway CO., Ltd., Chengdu, Sichuan 610031, China

Abstract: In this paper, a three-dimensional numerical simulation model is established based on smooth particle hydrodynamics (SPH) method. In this model, the dynamic behavior of debris flow is described by using the Bingham fluid model, and the bridge pier is regarded as the terrain condition. The repulsive force at the boundary is introduced to improve the boundary condition. Based on flume experiments, the accumulation processes of debris flow impacting the bridge pier with various viscosities and characteristics of the impact force-time curves are analyzed. The physical models are established, and the simulation of three-dimensional dynamic evolution processes of debris flow impacting the bridge pier with various rheological parameters and weights are realized. Moreover, the simulation results of the accumulation processes of debris flow with various rheological parameters and the impact force-time curves are analyzed. It is found that there are differences between the simulation results and the experimental results of the dynamic evolution processes of low-viscous debris flow impacting the bridge pier. From the view of fluid mechanics, the primary reason lies in the ignorance of the energy dissipation owing to lack of a description of Reynolds stresses caused by turbulence. Besides, the bridge pier safeguard procedures under the impact of debris flow with various viscosities are discussed. This work provides a theoretical support for further optimization of the three-dimensional numerical calculation model of debris flow impacting the bridge pier.
Keywords: SPH method; debris flow; bridge pier; impact; fluid-solid interaction

1 Introduction

In the mountainous areas of southwestern China, the constructed bridges are required to pass through debris flow ditches for the construction of roads and railways, which are directly threatened and damaged by debris flow disasters. For example, in Lianghe County, Yunnan Province on August 5, 2016, debris flow formed siltation on the upstream side of Zhangba Bridge, which eventually caused the villages to be buried and the bridge to collapse[1]. Besides, in Wenchuan County on July 10, 2013, the mass debris flow caused the collapse of several bridges, leading to serious damage and obstruction of the G213 Chengdu–Wenchuan Highway and Chengdu–Wenchuan Expressway[2]. With the construction of large-scale road projects such as the Sichuan-Tibet Railway and Chengdu–Lanzhou Railway, it is difficult for a large number of bridges to directly cross the debris flow ditches. The bridge piers are required to be arranged in the trench, which is directly threatened by the impact of debris flow. At the same time, the existence of bridge piers will have a significant impact on the dynamic evolution process of debris flow. Therefore, the investigation of the dynamic interaction process between bridge piers and debris flow plays a directive role in disaster prevention and mitigation of bridge engineering.

There are two key issues associated with the impact of debris flow on a bridge pier, one is the evolution characteristics of the impact force of the debris flow on the pier, and the other is the characteristics of flow around the pier after the debris flow impacts on the pier. Both issues involve complex fluid-structure interactions. To solve these problems, numerous research work has been done by a great number of scholars. For example, Cui et al.[3] analyzed the impact force of the viscous debris flow through the flume test, and discussed the influence of the Floyd number, density, and impact velocity. He et al.[4] analyzed the impact process of debris flow by using the fluid mechanics theory and the contact theory, and it was shown that the impact force was closely related to the solid volume fraction, particle material composition, movement speed, and depth of the debris flow. Moreover, He et al.[5–6] studied the impact characteristics of debris flow with different particle sizes, slurry viscosities, and solid-phase ratios through model tests, and the change laws of parameters such as the impact time history curve and load average value of debris flow were also analyzed. Wang et al.[7] conducted numerical simulations based on the characteristics of the impact force pulse signal of the debris flow and pointed out that the impact of large rocks was an important factor leading to structural damage.

Received: 29 July 2020 Revised: 28 December 2020
This work was supported by the Major Project of Science and Technology Research and Development Program of Ministry of Railways (Z2012-061), the Major Projects of the National Natural Science Foundation of China (41790433), the Special Experimental Project of China Railway (CLRQT-2015-012), the Research Project of China Railway (2012-major-3), the Key Deployment Projects of CAS (KFZD-SW-424) and the Key Research and Development Program of Sichuan Province (192DYF2709).
First author: LIANG Heng, male, born in 1991, PhD, Assistant Researcher, research interests: formation and evolution mechanism of landslide and debris flow, and numerical simulation method. E-mail: hliang@imde.ac.cn

Based on the modified Hertz contact theory and elasto-plastic theory, He et al.[8] analyzed the impact of large rocks on structures and found that a small impact velocity could cause the plastic failure of the contact surface. Furthermore, Jiang et al.[9] studied the impact force on the retaining wall by the flow of dry particles with different sizes and proposed the corresponding empirical formula for calculating the impact force considering the impact force and the static earth pressure. Gray et al.[10] used the depth average model to analyze the shock wave, stagnation point, and generated particle-free area when the particle flow impacts the obstacle and studied the problem of particulate matter flow around the pyramid structure. Cui et al.[11] used small-scale indoor experiments and numerical simulations to analyze the problems of particle flow around under supercritical gravity conditions. Longo et al.[12] discussed the problems of flow around for saturated particulate matter and pointed out that there was a clear difference between the pattern of flow around of the mixed media and model of flow around of the Newtonian fluid. Liu et al.[13] used the depth average model to analyze the detour characteristics of the debris flow impacting the bridge pier, and Liu et al.[14] also used the depth average model to simulate the flow characteristics around the pier after the impact of debris flow with various solid volume ratios. Additionally, Luo et al.[15] used LS-DYNA to analyze the impact of building blockage on the mobility of the landslide and its energy dissipation mechanism. Under the premise that the hazard-affected body is regarded as a topographical condition, Liu et al.[16] used the depth-averaged model to calculate the impact speed and depth of the hazard-affected body on the hazard-affected body. They calculated the impact force acting on the hazard-affected body by using the empirical formula. This force was regarded as a boundary condition to the hazard-affected body, and the collapse process of the hazard-affected body was analyzed. Besides, Feng[17] and Luo et al. [18] used a similar method to analyze the continuous collapse process of hazard-affected structures. The above studies usually consider the two key issues, the dynamic evolution process of debris flow and the impact force characteristics, separately, and ignore the two-way coupling effect of debris flow and structure. This results in a lack of dynamic analysis and three-dimensional simulation of the entire process of debris flow impacting the bridge pier based on fluid-solid interaction.

Regarding the issue above, we simulate and analyze the whole process of the debris flow impacting the bridge piers by using the smooth particle hydromechanics (SPH) method, based on the indoor flume model test of the debris flow impacting the bridge piers. The debris flow around characteristics with various rheological parameters and unit weights, as well as the time history evolution of impact force is analyzed. The experimental results and the simulation results are also compared and discussed. This work provides a theoretical basis for the simulation of the whole process of the debris flow impacting the bridge piers and provides theoretical support for more subsequent in-depth research.

2 SPH mathematical model

SPH method is a meshless method based on the Lagrangian description. The partial differential equations or integral equations are solved through a series of interaction points that carry material information, and it has been widely applied in computational fluid mechanics (CFD) and computational solid mechanics (CSM)[19-20]. Compared with the grid method, it has obvious advantages in the calculation of large deformation and free surface flow. Therefore, it has been widely used in the field of dynamic evolution simulation of landslides, debris flows, and other geological disasters[21–23].

2.1 The Bingham fluid model

Debris flow is a non-Newtonian fluid, whose mechanical properties are usually described by the Bingham fluid model[24]. The Bingham fluid model is given by

$$\boldsymbol{\sigma}^{\alpha\beta} = -p\delta^{\alpha\beta} + 2(\eta_{\mathrm{b}} + \frac{\tau_{\min}}{\dot{\gamma}})\dot{\boldsymbol{e}}^{\alpha\beta} \tag{1}$$

where p is the pressure; $\boldsymbol{\sigma}$ is the pressure tensor; $\delta^{\alpha\beta}$ is the Kronecker symbol; η_{b} is the viscosity coefficient of boundary particles; $\tau_{\min}$ is the yield stress; $\dot{\gamma}$ is the pure shear strain rate, and $\dot{\boldsymbol{e}}^{\alpha\beta}$ is the partial strain rate tensor. Superscripts α, β denotes the coordinate direction. The pure shear strain rate $\dot{\gamma}$ and the partial strain rate tensor $\dot{\boldsymbol{e}}^{\alpha\beta}$ are defined as

$$\dot{\gamma} = \sqrt{2\dot{\boldsymbol{e}}^{\alpha\beta}\dot{\boldsymbol{e}}^{\alpha\beta}} \tag{2}$$

$$\dot{\boldsymbol{e}}^{\alpha\beta} = \dot{\boldsymbol{\varepsilon}}^{\alpha\beta} - \frac{1}{3}\dot{\boldsymbol{\varepsilon}}^{\kappa\kappa}\delta^{\alpha\beta} \tag{3}$$

where $\dot{\boldsymbol{\varepsilon}}^{\kappa\kappa}$ is the volumetric strain rate, and $\dot{\boldsymbol{\varepsilon}}^{\alpha\beta}$ is the strain rate tensor, which is defined as:

$$\dot{\boldsymbol{\varepsilon}}^{\alpha\beta} = \frac{1}{2}(\frac{\partial \boldsymbol{v}^{\alpha}}{\partial x^{\beta}} + \frac{\partial \boldsymbol{v}^{\beta}}{\partial x^{\alpha}}) \tag{4}$$

where $\boldsymbol{v}^{\alpha}$, $\boldsymbol{v}^{\beta}$ are the velocities of the fluid; and x^{α}, x^{β} are coordinates of fluid.

In the calculation, the debris flow is regarded as a slightly compressible fluid, and the governing equation of the pressure is given by

$$p = B\left[(\frac{\rho}{\rho_0})^{\chi} - 1\right] \tag{5}$$

where B is a constant related to the artificial sound velocity of the fluid, whose value range is the same order of magnitude as the initial maximum pressure of the liquid phase; ρ is the fluid density; ρ_0 is the fluid density when $p = 0$; and χ is a constant, and its value is usually chosen as 7.

The key to using the Bingham fluid model is the calculation of the yield stress $\tau_{\min}$. Iverson deemed that the yield stress of debris flow is related to its normal stress and internal friction coefficient [25]. In this work, the Drucker-Prager criterion is applied to calculate the yield stress:

$$\tau_{\min} = -\mu p + c \tag{6}$$

where μ is the internal friction coefficient of debris flow; and c is the cohesion.

2.2 Fundamental theories of the SPH method

There are two key steps for the establishment of the SPH equations, the first one is the smooth approximation of kernel function, and the second one is the particle approximation of the kernel function equation. The smooth approximation of kernel function is the key of the SPH method, and the function $f(\boldsymbol{x})$ can be expressed as

$$\langle f(\boldsymbol{x})\rangle = \int_{\Omega} f(\boldsymbol{x}')W(\boldsymbol{x}-\boldsymbol{x}',h)\mathrm{d}\boldsymbol{x}' \tag{7}$$

And its derivative function is

$$\langle \nabla\cdot f(\boldsymbol{x})\rangle = -\int_{\Omega} f(\boldsymbol{x}')\cdot\nabla W(\boldsymbol{x}-\boldsymbol{x}',h)\mathrm{d}\boldsymbol{x}' \tag{8}$$

where $W(\boldsymbol{x}-\boldsymbol{x}',h)$ is a smooth kernel function, which needs to obey the regularization conditions, the Dirac function properties, and the compact conditions; h is the smooth length; $\boldsymbol{x}$ and $\boldsymbol{x}'$ are arbitrary three-dimensional coordinate vector and the three-dimensional coordinate vector of a given position, respectively. The particle approximation process of the kernel function equation is discretizing the study area into a series of particles that carries material information and then converting the integral form of the kernel function approximation into a discrete form of superposition and summation of particles in the support domain. Then, the particle approximate expression of the field function and its derivative at particle i can be written as

$$f(\boldsymbol{x}_i) = \sum_{j=1}^{N} f(\boldsymbol{x}_j)W(\boldsymbol{x}_i-\boldsymbol{x}_j,h)\frac{m_j}{\rho_j} \tag{9}$$

$$\nabla\cdot f(\boldsymbol{x}_i) = \sum_{j=1}^{N}\frac{m_j}{\rho_j} f(\boldsymbol{x}_j)\cdot\nabla_i W(\boldsymbol{x}_i-\boldsymbol{x}_j,h) \tag{10}$$

and:

$$\nabla W_i(\boldsymbol{x}_i-\boldsymbol{x}_j,h) = -\nabla W_j(\boldsymbol{x}_i-\boldsymbol{x}_j,h) = \frac{\boldsymbol{x}_i-\boldsymbol{x}_j}{r_{ij}}\frac{\partial W_{ij}}{\partial r_{ij}} \tag{11}$$

where the subscripts i, j are particle numbers; m_j is the mass of the particle j; ρ_j is the density of the particle j; and r_{ij} is the distance between particles.

Through integral approximation and particle approximation of the kernel function by the SPH method, the field function and its spatial derivative in the computational domain can be converted into a discretized summation format for any arrangement of particles in the support domain. Therefore, the background grid is not needed during the calculation of the SPH method, and the grid is not required for the connection between particles.

Debris flow is a viscous fluid [26], whose dynamic evolution process can be described by the three-dimensional Navier-Stokes (N-S) equation. The mass conservation equation and momentum conservation equation are given by

$$\frac{\mathrm{D}\rho}{\mathrm{D}t} = -\rho\frac{\partial \boldsymbol{v}^{\beta}}{\partial \boldsymbol{x}^{\beta}} \tag{12}$$

$$\frac{\mathrm{D}\boldsymbol{v}^{\alpha}}{\mathrm{D}t} = \frac{1}{\rho}\frac{\partial \boldsymbol{\sigma}^{\alpha\beta}}{\partial \boldsymbol{x}^{\beta}} + \boldsymbol{F}^{\alpha} \tag{13}$$

where $\boldsymbol{F}$ is the bulk stress component; t is time.

Considering the characteristics of the SPH method, an equation can be given by

$$\rho_i\sum_{j}^{N}\frac{m_j}{\rho_j}\boldsymbol{v}_i^{\beta}\cdot\frac{\partial W_{ij}}{\partial \boldsymbol{x}_i^{\beta}} = \rho_i\boldsymbol{v}_i^{\beta}\sum_{j}^{N}\frac{m_j}{\rho_j}\cdot\frac{\partial W_{ij}}{\partial \boldsymbol{x}_i^{\beta}} = 0 \tag{14}$$

where N is the number of particles in the support domain.

Inserting Eq.(12) into Eq.(10) and then substituting Eq. (10) into Eq.(14), we can obtain the SPH continuous density approximation equation of the velocity difference format. The continuous density equation of this format can effectively reduce the error caused by inconsistent particles, and it inserts the relative velocity into the continuity equation:

$$\frac{\mathrm{D}\rho_i}{\mathrm{D}t} = \rho_i\sum_{j=1}^{N}\frac{m_j}{\rho_j}\boldsymbol{v}_{ij}^{\beta}\frac{\partial W_{ij}}{\partial \boldsymbol{x}_i^{\beta}} \tag{15}$$

where $\boldsymbol{v}_{ij} = \boldsymbol{v}_i - \boldsymbol{v}_j$.

The first term on the right side of the Eq. (13) can be rewritten as

$$\frac{1}{\rho}\frac{\partial \boldsymbol{\sigma}^{\alpha\beta}}{\partial \boldsymbol{x}^{\beta}} = \frac{\partial}{\partial \boldsymbol{x}^{\beta}}\left(\frac{\boldsymbol{\sigma}^{\alpha\beta}}{\rho}\right) + \frac{\boldsymbol{\sigma}^{\alpha\beta}}{\rho^2}\frac{\partial\rho}{\partial \boldsymbol{x}^{\beta}} \tag{16}$$

Substituting Eq.(16) into Eq. (10), we can obtain the approximate formula of the SPH momentum conservation equation that reduces errors caused by inconsistent particles:

$$\frac{\mathrm{D}\boldsymbol{v}_i^{\alpha}}{\mathrm{D}t} = \sum_{j=1}^{N} m_j\left(\frac{\boldsymbol{\sigma}_i^{\alpha\beta}}{\rho_i^2} + \frac{\boldsymbol{\sigma}_j^{\alpha\beta}}{\rho_j^2}\right)\frac{\partial W_{ij}}{\partial \boldsymbol{x}_i^{\beta}} \tag{17}$$

2.3 Boundary condition of the SPH method

In the SPH method, there are commonly three rigid boundary conditions: repulsive boundary condition, virtual particle boundary condition, and dynamic boundary condition[27−28]. The dynamic boundary condition is superior to the repulsive boundary condition in terms of reducing particle defects at or near the boundary. Besides, it is easier to apply the numerical methods to the complex shape boundary compared with the virtual particle boundary condition[29]. Thus, the dynamic boundary condition is used in this work. The rigid boundary is expressed by multiple layers of fixed-position virtual particles, as shown in Fig. 1.

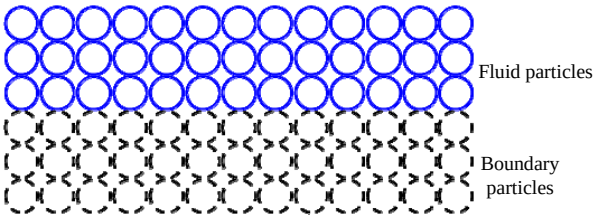

Fig. 1 Schematic diagram of the boundary condition

Except for the velocities and positions of the virtual particles, other field variables carried by the boundary virtual particles are involved in the calculation of the mass conservation equation and the momentum conservation equation.

2.4 Improvement of the boundary condition and time integration

The dynamic boundary condition is used in this work, and debris flow is regarded as a slightly compressible fluid. Re-initializing the density of boundary particles and fluid particles of debris flow at regular time steps can effectively reduce numerical oscillations. The equation of re-initialization is given by

$$\rho_i = \frac{\sum_j^N m_j W_{ij}}{\sum_j^N \frac{m_j}{\rho_j} W_{ij}} \tag{18}$$

As the boundary particles participate in the density re-initialization process, it is possible for them to penetrate the boundaries when the fluid particles are sparse. To prevent this process, a boundary repulsive force is introduced when particles penetrate the boundaries, which is given by

$$F_{\mathrm{re},ij} = \begin{cases} D_{\mathrm{r}}\left(\frac{l_0}{l_{ij}} - 1\right)\frac{\boldsymbol{x}_{ij}}{l_{ij}}, & l_{ij} < l_0 \\ 0, & l_{ij} \geqslant l_0 \end{cases} \tag{19}$$

where D_{r} is the repulsion coefficient; l_0 is the initial spacing for applying repulsive force; l_{ij} is the particle spacing. Compared with the strong repulsion model, the repulsive force in this method is relatively small. Only a weak force exists when the fluid particles reach a certain distance to the boundary particles, so the impact on calculations is slight. In the actual calculation process, the area where particles may penetrate is only located at the bottom surface of the water tank, which does not affect the impact process, and the application of a repulsive force will not affect the calculation results of an impact process.

Considering both the calculation speed and the calculation accuracy, the second-order precision Leap-Frog method is applied for time integration. The field variables and position information of the Leap-Frog method differ by half a time step. There are two steps of its calculation process, and the first one is given by

$$\left.\begin{aligned} \boldsymbol{X}\left(t + \frac{\Delta t}{2}\right) &= \boldsymbol{X}\left(t - \frac{\Delta t}{2}\right) + \Delta t \cdot \mathrm{D}\boldsymbol{X}(t) \\ \boldsymbol{x}(t + \Delta t) &= \boldsymbol{x}(t) + \Delta t \cdot \boldsymbol{v}\left(t + \frac{\Delta t}{2}\right) \end{aligned}\right\} \tag{20}$$

where $\boldsymbol{X}$ indicates field variables other than location information; Δt is the time step. As the position information and field variable information of the Leap-Frog method differ by half a time step, the field variable information needs to be moved back by half a time step to ensure the consistency of the particle position and the field variable information after each calculation step, which is given by

$$\boldsymbol{X}(t + \Delta t) = \boldsymbol{X}\left(t + \frac{\Delta t}{2}\right) + \frac{\Delta t}{2} \cdot \mathrm{D}\boldsymbol{X}(t) \tag{21}$$

The Bingham fluid model combined with the Drucker-Prager criterion, the improved boundary condition, and the *L-F* time integration method can be used to compile the calculation program for simulating the impact of the debris flow on bridges piers.

3 Debris flow impacting bridge pier tests

The Anxian–Hadapu section of the Chengdu–Lanzhou Railway is chosen as the research area, in which the railway passes through the Longmenshan fault zone, the Minjiang fault zone, and the West Qinling fold zone successively. It also straddles the Fujiang Rive, Tuojiang Rive, Minjiang Rive, and Bailongjiang River systems in the Yangtze River Basin, and traverses the Sichuan Basin, the Middle Mountain Valley and the Northwestern Sichuan Plateau. It needs to cross a large number of debris flow ditches. The existing specifications are not suitable for the calculation of railway piers. Thus, the laboratory model tests were conducted, which were used to validate the numerical simulations and to analyze the flow around as well as impact force evolution characteristics when a debris flow impacts the piers.

3.1 Platforms for indoor model tests

In order to study the dynamic response characteristics and flow around characteristics of the debris flow impacting the bridge pier, the model tests of debris flow impacting the bridge piers were conducted, using the test platform of Chengdu University of Technology[13, 30]. The model test platform for debris flow impacting the bridge piers is composed of debris flow troughs, hoppers, tailing pools, and test equipment, as shown in Fig. 2.

The width of the debris flow troughs is 0.35 m, the inclination angle of the No. 1 trough is 13.5°, and the inclination angle of the No. 2 trough is 6.5°. Besides, the height of No. 1 hopper is 8 m, and the height of No. 2 hopper is 5 m. During the test, the piezoresistive sensors were used to measure the impact force. The pier is cylindrical, which is fixed on the accumulation platform 0.50 m from the exit of the No. 2 trough by using angle steel. The sensor number and layout are shown in Fig. 3.

The debris flow materials used in the test were sampled from the debris flow ditches in the field. The designed diameter of the block stones in the debris flow is 4–6 cm, and the block stones were re-screened before all tests to maintain the consistency of particle gradation. For the source materials, the maximum particle size of block stones is 60 mm, and the minimum size is 0.25 mm. The gradation of block stone particles obtained by the screening test is shown in Fig. 4. The debris flow slurry is a suspension formed by mixing water and clay. The unit weight of the debris flow is 11–19 kN/m^3, and the volume fraction of block stones is less than 0.5 [30–31].

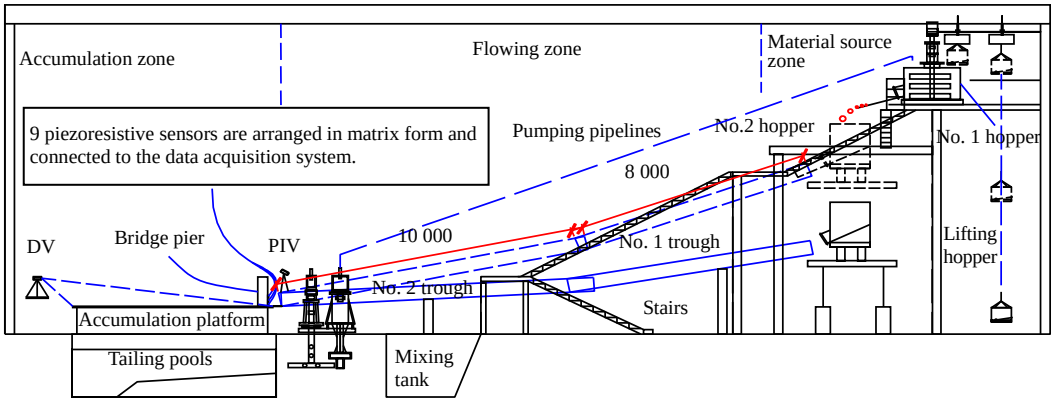

Fig. 2 Test platform for debris flow simulation (unit:mm)

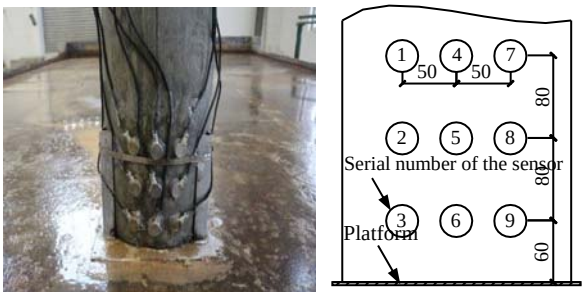

Fig. 3 Schematic diagram of the sensor layout(unit: mm)

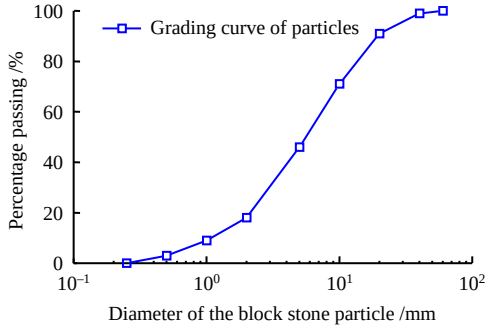

Fig. 4 Grading curve of block stone particles

3.2 Analysis of results

The research of Iverson et al.[32–34] and George et al.[35] shows that the fluidity of solid-liquid mixed media varies significantly with the volume fraction of the solid phase. In this test, the designed unit weight of the debris flow is 11–19 kN/m^3. According to the differences between the test phenomena, the debris flow is categorized into three types, including low-viscous debris flow, sub-viscous debris flow, and high-viscous debris flow. The unit weights of the three types of debris flows increase sequentially. The accumulation processes of the three types of debris flow are shown in Figs. 5–7.

Comparing Figs. 5, 6, and 7, there are obvious differences in the diffusion processes of the three types of debris flows after impacting the bridge piers. The mud quickly fills the blank area behind the pier after the low-viscous debris flow impacting the piers. As the debris flow impacts the sidewall of the platform, the waves are generated and the slurry flows back to the center of the platform. The solid-liquid mixture gradually spreads over the accumulation platform. The accumulation thickness is uniform and there is no obvious angle of repose. For sub-viscous debris flow, it expands to both sides as a whole after impacting the bridge piers. The spreading speed and spreading degree of mud behind the bridge piers are significantly lower than those of the low-viscous debris flow. For high-viscous debris flow, its fluidity after impacting the bridge piers is highly reduced. The debris flow fluid quickly converges behind the bridge pier, and there is a clear accumulation angle. With the increase of the viscosity of debris flow, it gradually turns from mud pooling at the piers into fluid accumulation behind the piers, which shows that the separation phenomenon of mud and block particles in the movement process is gradually reduced.

Under similar terrain conditions, the impact force of debris flow on the structure is mainly affected by the volume ratio of its solid phase, particle size, and slurry viscosity[36]. In addition, the characteristics of the time history curve of the impact force will change significantly with the increase of the viscosity of debris flow [6, 37–38]. In this test, the solid–liquid mixing method of debris flow is to directly blowdown from the hopper after mixing. The impact force signals of low-viscous debris flow and high-viscous debris flow are shown in Fig. 8.

(a) t=0.0 s (b) t=2.0 s (c) t=6.0 s

Fig. 5 Schematic diagram of an accumulation process of low-viscous debris flow

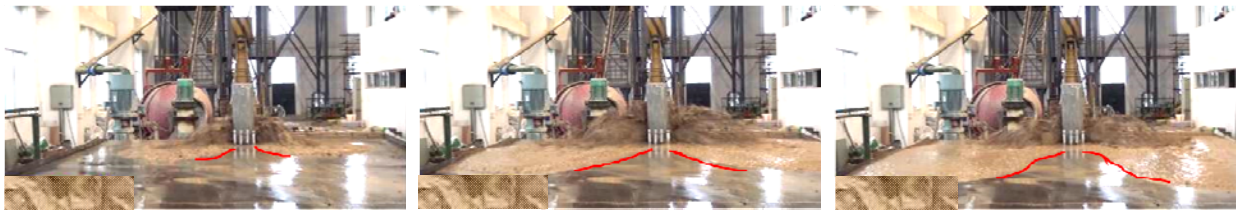

(a) t=0.0 s (b) t=1.0 s (c) t=5.0 s

Fig. 6 Schematic diagram of an accumulation process of sub-viscous debris flow

(a) t=0.0 s (b) t=2.0 s (c) t=6.0 s

Fig. 7 Schematic diagram of an accumulation process of high-viscous debris flow

The sensor may rebound during the measurement process, leading to negative measured values at some moments. These are normal measurement errors and do not affect the overall measurements. The impact force of debris flow is mainly composed of the impact force of large block stones and the continuous dynamic pressure of the slurry[3, 39]. Comparing Fig. 8(a) and Fig. 8(b), we can find that both low-viscous debris flow and high-viscous debris flow produce multiple peak shock signals, because of the discontinuity of the impact process. The peak impact force caused by the block stones is significantly larger than that caused by the slurry, and the frequency of the collection signal of the impact force of block stones is much smaller than that of the slurry, as the point load collection method is applied. Moreover, the continuous dynamic pressure generated by the slurry rises rapidly at the beginning and decreases slowly during the impact process. Besides, the fluctuations of the continuous dynamic pressure gradually decrease. Compared with the block stones, the impact process of the slurry is more continuous, which is more suitable for simulation by using continuum methods.

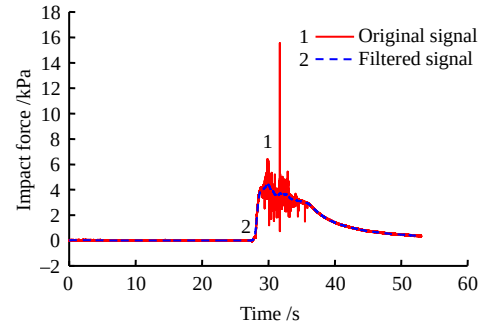

(a) Signals of impact force of low-viscous debris flow

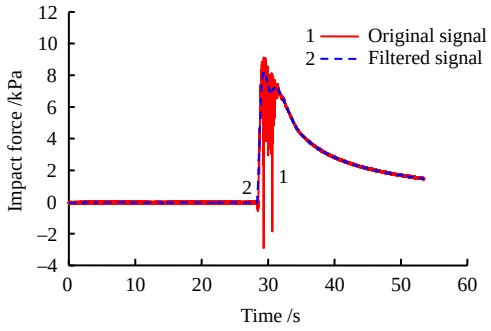

(b) Signals of impact force of high-viscous debris flow

Fig. 8 Signals of impact force of debris flow

4 Numerical simulation

4.1 Physical model for the numerical simulation

The main disadvantages of indoor model tests are long time and high cost. Thus, we construct a numerical model to simulate the impact process of debris flow on bridge piers based on the existing test results and compare the test results to validate the feasibility of the numerical model. The size of the stacking platform model is 3 m× 3 m, the pier diameter is 0.30 m, and the center of the bridge pier is 0.54 m from the outlet of the trough. Moreover, the width of the trough is 0.38 m, whose horizontal length is 3.5 m. The bottom inclination angle is 8.65°. Besides, the length of the water tank is 1.5 m, and the maximum elevation of fluid particles in the water tank is 1.44 m. The top surface of the fluid is flat. The constructed model is illustrated in Fig. 9.

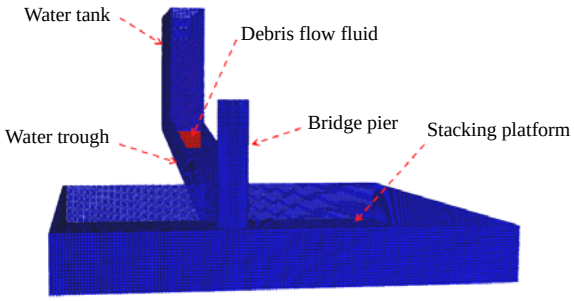

Fig. 9 Physical model of debris flow impacting bridge pier

The particle spacing is 0.01 m. The bridge piers are regarded as rigid boundaries, which are composed of three layers of particles. In addition, two layers of edge particles are set at the boundary. There are 137 998

particles in total, and the number of debris flow particles is 99503. As the Bingham model is used to describe the movement behavior of debris flow, the choice of the fluid viscosity coefficient and equivalent internal friction coefficient will affect the simulation results. According to our previous research of the sandpile collapse test and simulation[27], the fluidity of the solid–liquid two-phase medium increases with the volume fraction of the solid phase, as shown in Fig.10. H and L are the height and the length of the sandpile, respectively. d_s is the characteristic particle size of the sand pile.

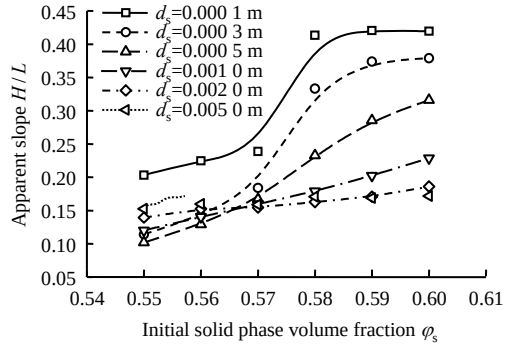

Fig. 10 Apparent slopes of sandpiles collapse with different initial volume fractions

As the volume fraction affects its final density, the equivalent friction coefficient can be reduced according to different densities. As the density decreases, the equivalent friction coefficient and viscosity coefficient in the calculation of the single-phase flow model decrease accordingly. The values of parameters in the simulation are chosen based both on the experiments and field experience, since the parameters of debris flow are complex. The equation of state is used to calculate the pressure of the debris flow. The parameters used in the numerical simulation are shown in Table 1.

Table 1 Material parameters

Number	Density /(kg • m^{-3})	Viscosity coefficient /(Pa • s)	Equivalent friction coefficient
#1	1 220	0.01	0.10
#2	1 440	0.10	0.12
#3	1 675	0.50	0.16
#4	1 910	1.00	0.22

4.2 Simulation of the accumulation process

The accumulation of debris flow is affected by its viscosity coefficient and friction coefficient. Different accumulation processes and stacked forms may occur. Compared with the test, no sensor is installed on the impact surface of the pier, leading to a difference between the shapes of the impact surfaces in the simulations and those in the test. The numerical results of different numbers are shown in Fig. 11.

As illustrated in Fig. 11, during the accumulation processes of debris flows No. 1 and No. 2, the debris flow spreads quickly to both sides after impacting the piers, and there is an obvious wave rolling phenomenon. During the diffusion processes, the width of the debris flow jet has a small change. After impacting the sidewalls of the accumulation platform, the debris flow flows back and converges on the accumulation platform, and finally fills the blank area behind the pier. The movement distance of the No. 3 debris flow is significantly reduced, and the speed of its front edge decreases rapidly after impacting the pier and spreading to both sides. Its diffusion shape is similar to a spindle with a wide center and narrow ends. Moreover, the angle between the inner side of the debris flow and the trough is rapidly reduced, and the debris flow gradually converges in the middle, filling the blank area downstream of the bridge pier. As for the No.4 debris flow which has a larger internal friction coefficient and viscosity coefficient, it spreads to both sides after impacting the pier. The speed of its front edge reduces sharply, and it converges quickly in the middle and fills the blank area downstream of the bridge pier.

Comparing Figs. 11(a)–11(d), it is found that there are clear differences between the flow around characteristics for debris flow with various friction coefficients and viscous coefficients, if the turbulence is not considered. The increase of the friction coefficient and the viscosity coefficient results in an increase of the resistance to the debris flow, which leads to a decrease in the length and width of the vacuum zone downstream of the pier. As a result, the accumulation process is changed and the accumulation range of debris flow is gradually shrinking. Besides, for different friction coefficients and viscosities, there are also obvious differences in the thickness distribution for the accumulation processes. Since the bottom surface of the physical model is flat and there exists the water tongue rolling phenomenon, the elevation of the fluid particles from the bottom surface is used to describe the change in the accumulation thickness during the impact process of the debris flow on the pier. The accumulation thicknesses of debris flows No. 1 and No. 4 at different time are chosen for comparison, as shown in Fig. 12.

From Fig.12, it is known that the rolling height of No. 1 debris flow caused by the impacting on the pier is significantly greater than that of No. 4 debris flow. The maximum rolling height of No. 1 debris flow exceeds 0.34 m. Before it impacts the sidewall, its thickness is relatively uniform as it moves. After it impacting the sidewall, a noticeable roll is produced and accumulation is generated near the sidewall. According to Fig.11, as the impact velocity decreases and the cap is completely accumulated by the debris flow, the pile of No. 1 debris flow at the outlet of the trough is fan-shaped. The maximum accumulation thickness is approximately 0.12 m, while the minimum thickness is around 0.06 m.

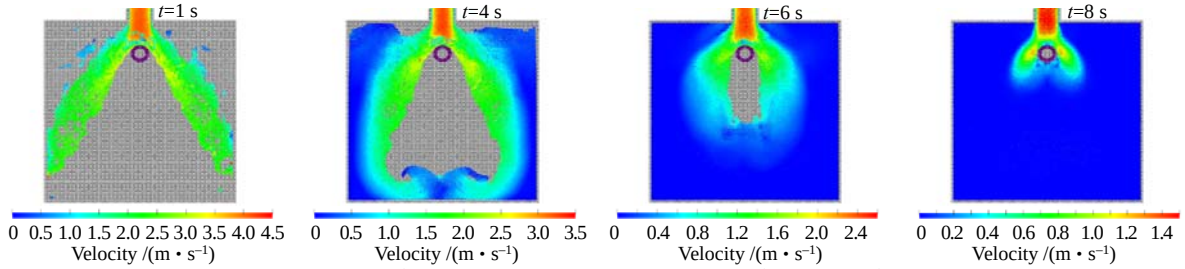

(a) Evolution of the accumulation process and the velocity of No. 1 debris flow

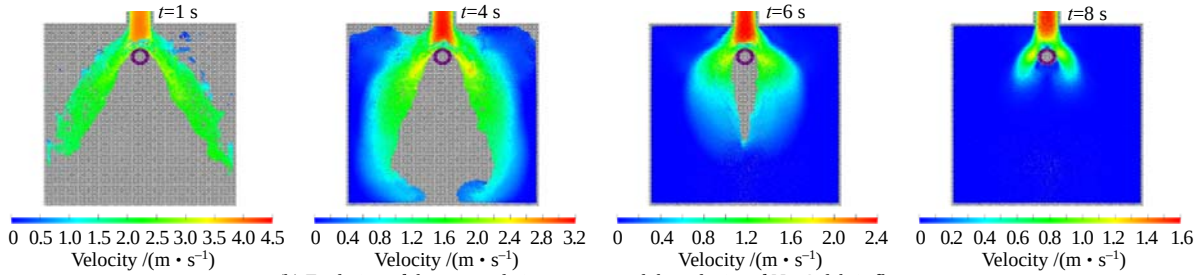

(b) Evolution of the accumulation process and the velocity of No. 2 debris flow

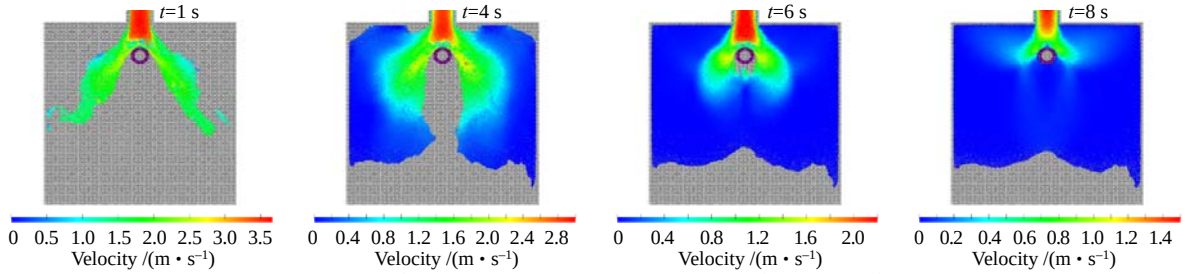

(c) Evolution of the accumulation process and the velocity of No. 3 debris flow

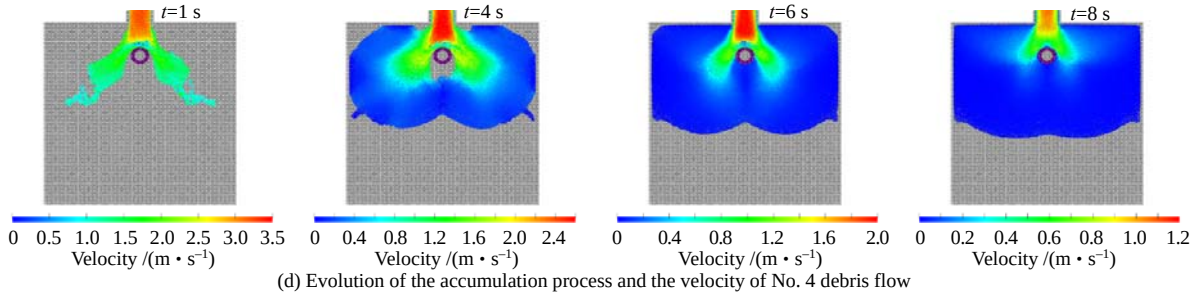

(d) Evolution of the accumulation process and the velocity of No. 4 debris flow

Fig. 11 Simulation results of accumulation processes for debris flow

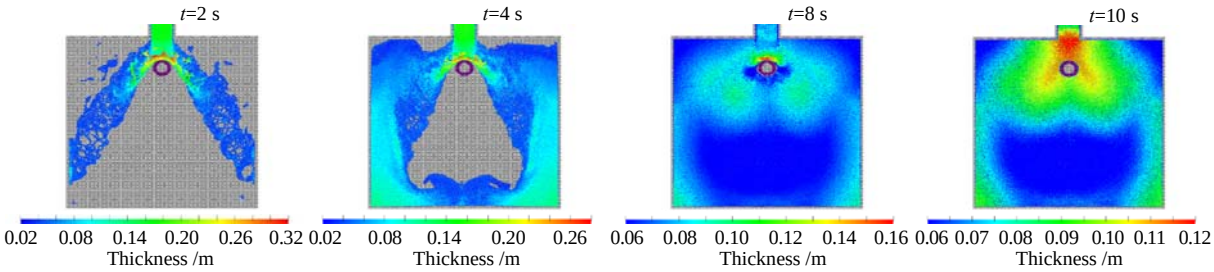

(a) Evolution of the accumulation thickness of No.1 debris flow

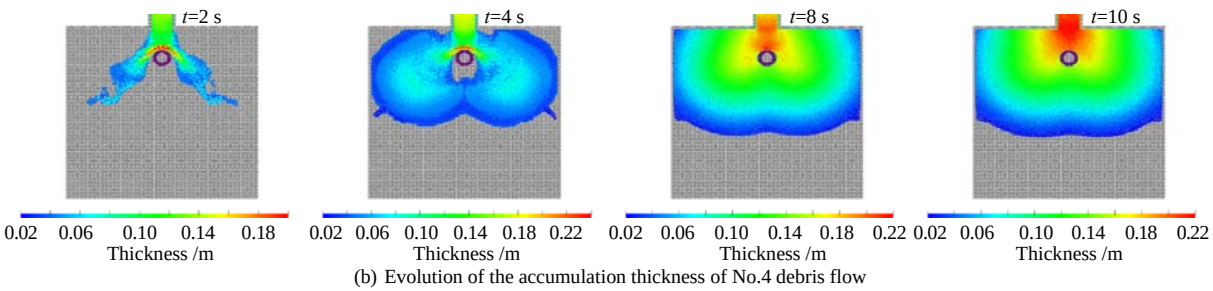

(b) Evolution of the accumulation thickness of No.4 debris flow

Fig. 12 Evolution of the accumulation thicknesses for debris flow

The maximum rolling height of No. 4 debris flow exceeds 0.26 m. The debris flow fanned out and the accumulation thickness gradually decreases outward from the point of impact. At t=10 s, the maximum accumulation thickness is approximately 0.22 m, and the minimum thickness is 0.02 m. Comparing Figs. 12 (a) and (b), we can find that the pile shape of debris flow is mainly fan-shaped at a low impact velocity. Under the high impact velocity condition, however, there will be significant differences in the thickness and shape of the pile for various friction coefficients and viscosity coefficients.

4.3 Analysis of impact force evolution processes

The SPH method is a method of integral interpolation. According to Newton's third law, the force is calculated using the following equation:

$$\boldsymbol{F}_{\mathrm{s}} = -\sum_{i=1}^{M} m_i \sum_{j=1}^{N} m_j \left(\frac{\sigma_i^{\alpha\beta}}{\rho_i^2} + \frac{\sigma_j^{\alpha\beta}}{\rho_j^2}\right) \frac{\partial W_{ij}}{\partial \boldsymbol{x}_i^{\beta}} \tag{22}$$

where $\boldsymbol{F}_{\mathrm{s}}$ is the impact force of debris flow on the pier, the subscript i represents the particle number of the debris flow fluid, the subscript j represents the number of the pier particle. According to the characteristics of the SPH method, the formula for calculating the average velocity of the debris flow impacting the bridge pier is given by

$$\boldsymbol{v}_{\mathrm{s}} = \frac{\sum_{i=1}^{M}\sum_{j=1}^{N} \frac{m_j}{\rho_j} \boldsymbol{v}_j W_{ij}}{\sum_{i=1}^{M}\sum_{j=1}^{N} \frac{m_j}{\rho_j} W_{ij}} \tag{23}$$

where i and j are the particle numbers of debris flow; $\boldsymbol{v}_j$ is the velocity of the fluid particles; and $\boldsymbol{v}_{\mathrm{s}}$ is the average impact velocity. The sampling frequency of force and impact velocity is 1000 Hz. The time–history curve and filter curve of the force and impact velocity of the debris flow with different viscosity coefficients and friction coefficients on the impact surface of the pier are displayed in Fig. 13.

From Fig. 13, it is shown that the impact velocity in the direction of the impact surface decreases rapidly after the debris flow impacts the pier. Comparing with Fig. 8, we can find that the simulation results of the impact force-time history curve can reflect the evolution characteristics of the impact force accurately when the debris flow impacts the bridge pier. The impact force of No. 1 debris flow on the impact surface of the pier increases first and then reduces, and finally reaches a steady state. At this time, the static earth pressure of the debris flow on the impact surface of the pier is about 20 N. Moreover, the time history curve of the impact force of the No. 4 debris flow on the impact surface of the bridge pier has a concave section at the initial stage. The impact force reduces at first before increasing and reaching the peak, and the impact force of the debris flow on the impact surface of the pier is about 106 N when a final steady state is reached. Furthermore, the impact time history curves of No. 2 and No. 3 debris flow are in the transitional state as aforementioned, and the static earth pressure is about 35 N and 73 N, respectively. Without considering the impact of large block stones, the impact force of debris flow is mainly affected by the dynamic impact pressure and the static earth pressure. The dynamic impact pressure is mainly dominated by the unit weight, impact velocity, and the Frode number. With the increase of the unit weight, friction coefficient, and viscosity coefficient of the debris flow, the impact velocity decreases, leading to a smaller Frode number and a larger accumulation

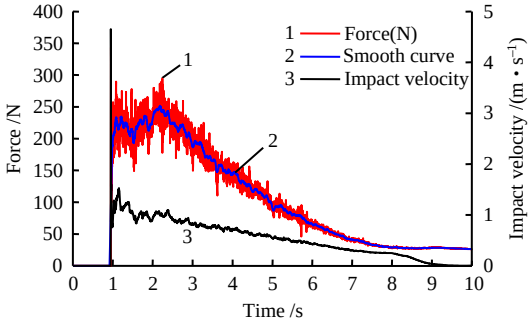

(a) No.1 debris flow

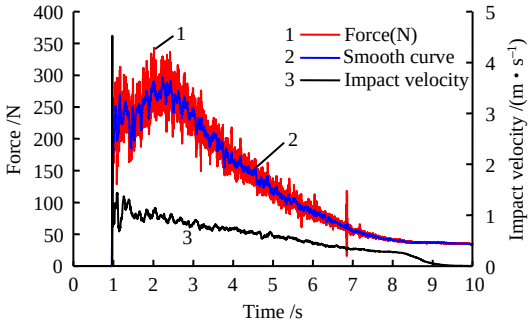

(b) No.2 debris flow

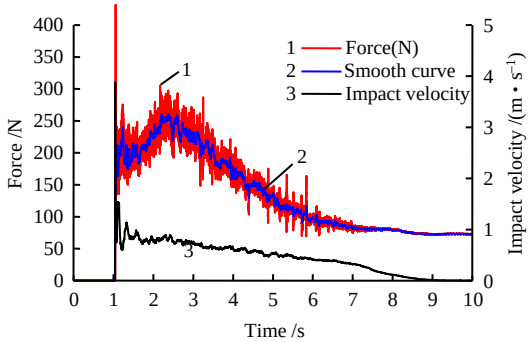

(c) No.3 debris flow

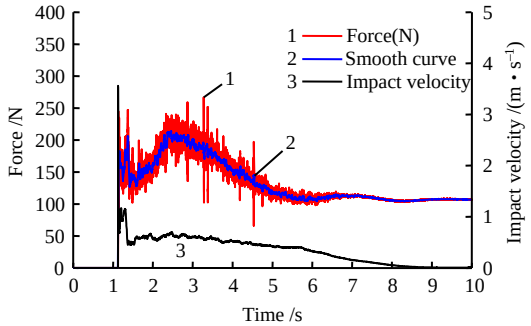

(d) No.4 debris flow

Fig. 13 Simulations results of impact force–time curves

thickness. Additionally, the peak force of the debris flow on the impact surface of the pier increases at first and then reduces, while the static earth pressure increases obviously.

5 Discussions

As the test parameters are difficult to determine, the values of these parameters are chosen based on experience. The debris flow is deemed as an incompressible fluid. Based on the depth average theory of the momentum conservation equation[40], the density item in the pressure and friction items can finally be deleted, and the viscous resistance term is the key factor of the momentum. The maximum velocity of the debris flow in the simulation is less than 5 m/s, and the thickness is about 0.15 m. As a result, the friction resistance term is at the magnitude of 10^3, and the maximum viscous resistance term is at the magnitude of 10^1. Therefore, the deviation of the density values has only a slight effect on the results, and the dynamic behaviors of debris flows with various unit weights mainly depend on the values of the equivalent friction coefficient and the viscosity coefficient.

By comparing the test results with the simulation results, it is found that with the increase of the friction coefficient and the viscous coefficient, the agreement between the experimental results and the numerical results of the dynamic evolution process of the debris flow impacting the bridge piers has gradually improved. In fluid mechanics, there are two flow states during the motion of the viscous fluid, namely laminar flow and turbulent flow. Turbulence can be distinguished by the lower critical Reynolds number and the upper critical Reynolds number. The Reynolds number is given by

$$Re = \frac{v_0 \rho L_0}{\mu} \tag{24}$$

where v_0 and L_0 are the movement speed and the smooth characteristic length of debris flow, respectively.

Commonly, the upper Reynolds number is chosen as 13800, and the lower Reynolds number is 2320. When the unit weight of the debris flow is small, there will be an obvious solid–liquid separation phenomenon. The relative flow between liquid and solid phases will be obvious, and the flow state of the liquid phase can be distinguished based on the Reynolds number. According to the depth and movement speed of the debris flow in the water trough in the test, the equation for the Reynolds number range of the debris flow in the flume is given by

$$\frac{236.309}{\mu} \leqslant Re \leqslant \frac{2\ 740.736}{\mu} \tag{25}$$

Under the extreme condition of a lower Reynolds number, turbulence will occur when the viscosity coefficient of the liquid phase of the debris flow reaches 0.102 Pa·s, and it will be completely in a turbulent state when the viscosity coefficient is less than 0.017 Pa·s. Besides, under the extreme condition of an upper Reynolds number, turbulence will occur when the viscosity coefficient of the liquid phase is as low as 1.181Pa·s, and it will reach the complete turbulent state when the viscosity coefficient is less than 0.199 Pa·s. In the physical model test of debris flow, the speed of the liquid phase of the low-unit weight debris flow tends to be larger, leading to a lower viscosity coefficient and a larger liquid phase volume fraction. As a result, it is easier for turbulence to occur. According to the Reynolds average motion equation, the Reynolds stress caused by the pulsation should be considered in the turbulent state. The shear stress of the Bingham fluid model can be divided into friction terms and viscous terms. The viscosity term is established based on the laminar flow assumption, which ignores the Reynolds stress. This leads to the low viscous dissipation of the liquid phase in the low-unit weight debris flow if turbulence is not considered. As a result, the energy dissipation of the liquid phase after impact will be relatively small, and the diffusion rate of the liquid phase tends to be large. This makes it difficult to model the slurry dispersion in the physical model test by using the simulation results of the low-unit weight debris flow which is described by the Bingham fluid model. However, comparing the overall simulation results and test results, it can be found that the single-phase flow model can well simulate the movement and accumulation process of the solid–liquid mixed fluid in the physical model test. In addition, for high-unit weight debris flow, the numerical simulation results are in good agreement with the physical model test results.

After the debris flow impacts the bridge pier, a critical state is reached, and the laminar flow state can be changed to the turbulent flow state. The movement speed and the flow around process will also be changed obviously, which can highly affect the scour process at the foundation of the bridge pier and the flow around process behind the bridge pier. For the low-viscous debris flow, the erosion intensity of the pier foundation can be greatly boosted in the direction of the pier's impact surface under the turbulent state. At the same time, the scope of the vacuum area behind the piers is reduced and the erosion of the pier foundation is exacerbated. For the viscous debris flow, accumulation may occur around the bridge piers and block bridges and culverts, leading to insufficient cross-sections for clearance and drainage. Thus, the drainage capacity is reduced, the debris flow may overflow and the silt may bury the bridges and culverts. Therefore, in addition to setting up suitable anti-collision structures and drainage projects, the pier foundations should be strengthened for bridges crossing low-viscous debris flow ditches. For bridges that span viscous debris flow ditches, sufficient free space should be reserved to avoid the blockage of the bridges and culverts and the burial of the bridge decks.

6 Conclusions

By comparing with the laboratory trough test results of the debris flow impacting the bridge piers, we validate

that the Bingham fluid model and the improved SPH method can be used to simulate the impact of debris flow on bridge piers. By the in-depth analyses and discussions of the test and simulation results, the conclusions can be obtained as follows:

(1) The impact force generated by debris flow and block stones is significantly higher than that generated by slurry. The frequency of the impact force signal of the block stones is much lower than that of the slurry obtained by the point load collection method.

(2) With the increase of the viscosity of the debris flow, the solid–liquid separation phenomenon of the block stone and the slurry gradually weakens after the debris flow impacts the bridge pier, and its stacked form is also markedly changed.

(3) Embedding the Bingham fluid model into a three-dimensional calculation model based on the SPH method can simulate the velocity and depth evolution of the debris flow after impacting the pier, and the impact time history curve can be obtained. According to the simulation results, the peak impact force of the debris flow on the bridge piers increases at first and then reduces, as the viscosity and the unit weight of the debris flow increase.

(4) Bingham model and the SPH method can be used to simulate the two-way coupling effect between the debris flow and bridge piers, as well as the three-dimensional motion process of debris flow. Especially, the impact process of viscous debris flow on the bridge pier can be simulated very well. However, it is difficult to model the spreading process of the low-viscous debris flow at the piers, since the turbulence effect is not considered.

(5) For bridges across the debris flow ditches, in addition to conventional debris flow anti-collision structure and drainage engineering, the bridge pier foundation needs to be strengthened and the height of the reserved airside surface needs to be verified, according to the characteristics of the debris flow ditches.

References

[1] WANG Ling, LIU Zhen, YANG Lin, et al. Analysis for the disaster mechanism of Zhangba river “8.5” mudslide in Lianghe county, Yunnan province[J]. Journal of Geological Hazards and Environment Preservation, 2017, 28(4): 22–25.

[2] JIANG Xian-gang, GE Yong-gang, LEI Yu, et al. The failure mechanism of Maojiawan bridge by “7·10” debris flow[J]. Mountain Research, 2015, 33(3): 311–317.

[3] CUI P, ZENG C, LEI Y, et al. Experimental analysis on the impact force of viscous debris flow[J]. Earth Surface Processes and Landforms, 2015, 40(12): 1644–1655.

[4] HE S, LIU W, LI X. Prediction of impact force of debris flows based on distribution and size of particles[J]. Environmental Earth Sciences, 2016, 75(4): 298.

[5] HE Xiao-ying, CHEN Hong-kai, TANG Hong-mei, et al. Experimental study on impacting characteristics of debris flow heads[J]. Journal of Chongqing Jiaotong University (Natural Sciences), 2014, 33(1): 85–89.

[6] HE Xiao-ying, TANG Hong-mei, CHEN Hong-kai. Experimental study on impacting characteristic of debris flow considering different slurry viscosities, solid phase ratios and grain diameter[J]. Chinese Journal of Geotechnical Engineering, 2014, 36(5): 977–982.

[7] WANG Xiu-li, HUANG Zhao-sheng. Dynamic response analysis of the new debris flow block under impact load[J]. The Chinese Journal of Geological Hazard and Control, 2013, 24(4): 61–65.

[8] HE Si-ming, LI Xin-po, WU Yong. Calculation of impact force of outrunner blocks in debris flow considering elastoplastic deformation[J]. Chinese Jounal of Rock Mechanics and Engineering, 2007, 26(8): 1664–1669.

[9] JIANG Y, ZHAO Y, TOWHATA I, et al. Influence of particle characteristics on impact event of dry granular flow[J]. Powder Technology, 2015, 270: 53–67.

[10] GRAY J, TAI Y C, NOELLE S. Shock waves, dead zones and particle-free regions in rapid granular free-surface flows[J]. Journal of Fluid Mechanics, 2003, 491: 161–181.

[11] CUI X, GRAY J. Gravity-driven granular free-surface flow around a circular cylinder[J]. Journal of Fluid Mechanics, 2013, 720: 314–337.

[12] LONGO S, VALIANI A, LANZA l, et al. Experimental study of the grain-water mixture flow past a cylinder of different shapes[J]. European Journal of Mechanics-B/ Fluids, 2013, 38: 101–113.

[13] LIU Fa-ming, WANG Dong-po, HE Si-ming, et al. Numerical simulation and experiment analyses of debris flow movement around bridge pier[J]. Mountain Research, 2018, 36(4): 571–580.

[14] LIU W, HE S. Simulation of two-phase debris flow scouring bridge pier[J]. Journal of Mountain Science, 2017, 14: 2168–2181.

[15] LUO H Y, SHEN P, ZHANG L M. How does a cluster of buildings affect landslide mobility: a case study of the Shenzhen landslide[J]. Landslides, 2019, 16(12): 2421–2431.

[16] LIU W, YAN S, HE S. Landslide damage incurred to buildings: a case study of Shenzhen landslide[J]. Engineering Geology, 2018, 247: 69–83.

[17] FENG S, GAO H, GAO L, et al. Numerical modeling of interactions between a flow slide and buildings considering the destruction process[J]. Landslides, 2019, 16(10): 1903–1919.

[18] LUO H Y, ZHANG L L, ZHANG L M. Progressive failure of buildings under landslide impact[J]. Landslides, 2019, 16(7): 1327−1340.

[19] LIU G R, LIU M B. Smoothed particle hydrodynamics: a mesh free particle method[M]. Singapore: World Scientific, 2003.

[20] LIU M B, LIU G R. Smoothed particle hydrodynamics (SPH): an overview and recent developments[J]. Archives of Computational Methods in Engineering, 2010, 17(1): 25−76.

[21] HUANG Y, DAI Z, ZHANG W, et al. Visual simulation of landslide fluidized movement based on smoothed particle hydrodynamics[J]. Natural Hazards, 2011, 59(3): 1225−1238.

[22] DAI Z, HUANG Y, CHENG H, et al. 3D numerical modeling using smoothed particle hydrodynamics of flow-like landslide propagation triggered by the 2008 Wenchuan earthquake[J]. Engineering Geology, 2014, 180: 21−33.

[23] LIANG H, HE S, LEI X, et al. Dynamic process simulation of construction solid waste (CSW) landfill landslide based on SPH considering dilatancy effects[J]. Bulletin of Engineering Geology and the Environment, 2019, 78(2): 763−777.

[24] WANG Yu-yi, JAN Chyan-deng, YAN Bi-yu. Debris-flow rheology and movement[M]. Changsha: Hunan Science and Technology Press, 2014.

[25] IVERSON R M. The physics of debris flows[J]. Reviews of Geophysics, 1997, 35(3): 245.

[26] YE Bin, HUANG Yu, YE Wei-min, et al. The impact force of debris flow on structures using SPH method[J]. Journal of Catastrophology, 2010, 25(Suppl.1): 380−380.

[27] CRESPO A J C, GOMEZ-GESTEIRA M, DALRYMPLE R A. Boundary conditions generated by dynamic particles in SPH methods[J]. Computers, Materials and Continua, 2007, 5(3): 173−184.

[28] LIU M B, SHAO J R, CHANG J Z. On the treatment of solid boundary in smoothed particle hydrodynamics[J]. Science China (Technological Sciences), 2012, 55(1): 244−254.

[29] LIANG H, HE S, CHEN Z, et al. Modified two-phase dilatancy SPH model for saturated sand column collapse simulations[J]. Engineering Geology, 2019, 260, 105219.

[30] WANG Dong-po, CHEN Zheng, HE Si-ming, et al. Physical model experiments of dynamic interaction between debris flow and bridge pier model[J]. Rock and Soil Mechanics, 2019, 40(9): 3363−3372.

[31] WANG D P, CHEN Z, HE S M, et al. Measuring and estimating the impact pressure of debris flows on bridge piers based on large-scale laboratory experiments[J]. Landslides, 2018, 15(7): 1331−1345.

[32] IVERSON R M. Regulation of landslide motion by dilatancy and pore pressure feedback[J]. Journal of Geophysical Research-Earth Surface, 2005, 110(F2).

[33] IVERSON R M, GEORGE D L. A depth-averaged debris-flow model that includes the effects of evolving dilatancy. I. physical basis[J]. Proceedings of the Royal Society A—Mathematical Physical and Engineering Sciences, 2014, 470(2170): 20130819.

[34] IVERSON R M, REID M E, IVERSON N R, et al. Acute sensitivity of landslide rates to initial soil porosity[J]. Science, 2000, 290(5491): 513−516.

[35] GEORGE D L, IVERSON R M. A depth-averaged debris-flow model that includes the effects of evolving dilatancy. II: numerical predictions and experimental tests[J]. Proceedings of the Royal Society A—Mathematical Physical and Engineering Sciences, 2014, 470 (2170): 20130820.

[36] WANG You-biao, YAO Chang-rong, LIU Sai-zhi, et al. Experimental study of debris flow impact forces on bridge piers[J]. Rock and Soil Mechanics, 2019, 40(2): 616−623.

[37] CHEN Hong-kai, TANG Hong-mei, XIAN Xue-fu, et al. Probability distribution features of fluctuating impact force of debris flow[J]. Journal of Vibration and Shock, 2010, 29(8): 124−127.

[38] HE Xiao-ying, TANG Hong-mei, ZHU Xiu-zhu, et al. Tests for impacting characteristics of debris flow slurry[J]. Journal of Vibration and Shock, 2013, 32(24): 127−134.

[39] ZENG Chao, SU Zhi-man, LEI Yu, et al. An experimental study of the characteristics of impact forces between debris flow slurry and large-sized particles[J]. Rock and Soil Mechanics, 2015, 36(7): 1923−1930.

[40] SAVAGE S B, HUTTER K. The motion of a finite mass of granular material down a rough incline[J]. Journal of Fluid Mechanics, 1989, 199: 177−215.